

## Article

# Coupled Monte Carlo and Thermal-Hydraulics Modeling for the Three-Dimensional Steady-State Analysis of the Xi'an Pulsed Reactor

Duoyu Jiang <sup>1,2,\*</sup> , Peng Xu <sup>1</sup>, Tianliang Hu <sup>2</sup>, Xinbiao Jiang <sup>2</sup>, Lipeng Wang <sup>2</sup>, Da Li <sup>2</sup>, Xinyi Zhang <sup>2</sup> and Lu Cao <sup>2</sup><sup>1</sup> Xi'an Research Institute of Hi-Tech, Xi'an 710025, China<sup>2</sup> Northwest Institute of Nuclear Technology, Xi'an 710024, China; hutianliang1990@stu.xjtu.edu.cn (T.H.); wang.0214@stu.xjtu.edu.cn (L.W.); zxy0501@stu.xjtu.edu.cn (X.Z.); new40521@stu.xjtu.edu.cn (L.C.)

\* Correspondence: yu112200@alumni.sjtu.edu.cn

**Abstract:** The Xi'an Pulsed Reactor (XAPR) is characterized by its small core size and integrated fuel moderator structure, which results in a non-uniform core power and temperature distribution. Consequently, a complex coupling relationship exists between its core neutronics and thermal hydraulics, necessitating the assurance for the operational safety of the XAPR. To optimize the experimental scheme in the reactor, a refined three-dimensional steady-state nuclear-thermal coupling analysis is imperative. This study focuses on investigating the coupling calculation of a three-dimensional steady-state neutronics and thermal-hydraulics model for the XAPR by utilizing an open-source multi-physical coupling framework known as Cardinal. The neutron transport equation is effectively solved using OpenMC, while a three-dimensional heat conduction model is employed to compute the heat conduction of the fuel elements. Furthermore, a parallel multi-channel model is utilized to determine the fluid heat transfer. The research is centered on the XAPR, whereby Monte Carlo and thermal-hydraulics coupling calculations of the core under steady-state full-power conditions are conducted, specifically at an operational capacity of 2 MW. The results demonstrate a strong agreement between the simulation and experimental outcomes. The maximum temperature recorded for the thermometric fuel element in the XAPR is 795.1 K, with a deviation of approximately  $-5.7\%$  from the measured value. Moreover, the outlet fluid temperature of the thermal channel is observed to be 360 K, exhibiting a deviation of around  $-2.7\%$  from the measured value.

**Keywords:** Xi'an Pulsed Reactor; nuclear reactor physics; reactor thermal-hydraulics; multi-physics coupling



**Citation:** Jiang, D.; Xu, P.; Hu, T.; Jiang, X.; Wang, L.; Li, D.; Zhang, X.; Cao, L. Coupled Monte Carlo and Thermal-Hydraulics Modeling for the Three-Dimensional Steady-State Analysis of the Xi'an Pulsed Reactor. *Energies* **2023**, *16*, 6046. <https://doi.org/10.3390/en16166046>

Academic Editor: Alessandro Del Nevo

Received: 17 July 2023

Revised: 7 August 2023

Accepted: 14 August 2023

Published: 18 August 2023



**Copyright:** © 2023 by the authors. Licensee MDPI, Basel, Switzerland. This article is an open access article distributed under the terms and conditions of the Creative Commons Attribution (CC BY) license (<https://creativecommons.org/licenses/by/4.0/>).

## 1. Introduction

Due to the substantial generation of radioactive materials during the operation of the reactor, the ensuing interaction between these radioactive substances and environmental media is predicted to yield consequential adverse effects [1–3], thereby necessitating a meticulous scrutiny of reactor safety. The reactor system encompasses a plethora of physical processes, such as neutron transport, flow heat transfer, and structural deformation, which all intricately interact with one another and ultimately govern the reactor's state. Situated within a densely populated city, the Xi'an Pulse Reactor (XAPR) warrants the establishment of a precise multi-physical coupling model to ensure its operational safety, as well as to consequently safeguard the well-being of the surrounding population and environment.

The XAPR, a uranium hydrogen pulse reactor of the swimming pool type, employs a fuel-rod structure that is characterized by its coarseness, allowing for natural convection heat transfer between the fuel rods and the coolant. Its primary circuit functions on an open force cycle [4]. Notably, the XAPR exhibits distinct traits such as a compact core size, an integrated fuel moderator structure, and an uneven distribution of power and temperature within the core. Consequently, this configuration engenders a complex interplay among

the parameters that span different physical fields, including the neutron physical field, fuel temperature field, and coolant temperature field, among others. The intricate coupling relationship between the core neutronics and thermal hydraulics further complicates matters. Presently, our understanding of the multi-physical coupling phenomenon in the context of the XAPR remains limited, thus prompting the utilization of equivalent parameters or average channel models in the computation of neutron and thermal hydraulics. To enhance the accuracy of steady-state simulations for the XAPR, one viable approach lies in the adoption of a three-dimensional neutron-thermal-hydraulic coupling analysis method. This methodology holds significant practical value as it contributes to the optimization of the experimental scheme for the XAPR, and it guarantees its safe operation within steady-state conditions.

In recent years, extensive research has been conducted on the steady-state operation of the XAPR, and these primarily fall into two main categories. The first category involves individual neutronics or thermal-hydraulics calculations. Neutronics calculations utilize methods such as the Monte Carlo method and deterministic methods. The core modeling of the XAPR is accomplished through the implementation of a MCNP. Building on this, a Monte Carlo deep penetration coupled shielding method was developed for the thermal neutron source design of the XAPR [5]. A burnup analysis of the XAPR was carried out using MCNP and WIMS programs [6]. Detailed calculations of the steady-state parameters of the XAPR were performed via a thermal and hydraulic design program system that was developed by the Nuclear Power Institute of China [7]. Furthermore, the thermal and hydraulic parameters for the steady-state core layout of the XAPR's first cycle were determined with the code PRTHA [8]. The second category encompasses neutronics and thermal-hydraulics coupling calculations. Zhao et al. [9] developed a coupling code for the neutron space-time dynamics and thermal hydraulics in pulse reactors. This calculation not only analyzes the steady neutron flux, but also examines the temperature distribution of the fuel rod in pulse parameter calculations for the XAPR. An additional coupling calculation method was established, thereby employing the neutron transport code Daisy in conjunction with single-channel thermal hydraulics. This method facilitates the calculation of steady-state nuclear thermal coupling [10].

Despite these advancements, several issues persist. Firstly, neutronics or thermal-hydraulics calculations that are conducted in isolation fail to consider the interaction and coupling effects of the core, thus inadequately reflecting the actual operational processes of the XAPR. Secondly, existing nuclear-thermal coupling calculations rely on deterministic codes to facilitate the coupling process. However, this approach necessitates the establishment of multi-group or few-group cross-sections for neutron calculations, thus leading to significant approximations.

This paper presents a three-dimensional analysis of the steady-state nuclear-thermal coupling of the XAPR, wherein the core power, temperature, and coolant temperature distribution are simulated. Specifically, the coupling effect of neutronics, solid heat conduction, and fluid heat transfer when the XAPR is under a 2 MW steady-state condition was investigated. The neutron calculations were performed using OpenMC [11,12], which relied on the continuous point cross-sections. The heat conduction calculations, on the other hand, were based on the MOOSE [13,14], employing the continuous finite element method. The conventional thermal-hydraulic calculations traditionally rely on the finite volume method (FVM) or the finite difference method (FDM). Although the FDM theory is well established and the method is straightforward, it presents challenges in processing irregular areas. On the other hand, the FVM is suitable for fluid calculations and demonstrates proficiency in handling irregular geometries, yet its precision is no more than that of the second order. In this study, the finite element method (FEM) was employed to address the thermal-hydraulic predicaments encountered in the context of the XAPR. The principal rationale behind this choice lies in the FEM's robust geometric adaptability, Jacobian matrix structure specification, modularity for programming, and its potential for large-scale parallel computation. However, it should be noted that the FEM necessitates

significant memory and computational resources, often requiring appropriate acceleration methods for its efficient implementation. In this paper, the direct coupling of neutronics with thermal-hydraulic calculations was achieved, and an internal coupling iterative calculation of the multi-physical model was realized within the Cardinal framework [15,16]. This approach not only harnessed the advantages of the Monte Carlo method in solving the neutron transport equation, but also accounted for the characteristics of the deterministic method in addressing thermal-hydraulic problems.

This paper is structured into five sections. Section 1 provides an introduction, outlining the background and current research status. In Section 2, the fundamental aspects of the XAPR are presented. The calculation model and the scheme for neutronics and thermal-hydraulics coupling are elaborated upon in Section 3. Section 4 presents the numerical results obtained from the analysis. Finally, in Section 5, the paper concludes by summarizing the findings and proposing avenues for future research.

## 2. Description of the XAPR

The XAPR device comprises three main components: the reactor core, the reactor main system, and the experimental device (which functions as a small pool-type research reactor, as well as utilizes uranium hydrogen as fuel and graphite as a reflective layer). The cooling water system employed is an open system, and the coolant system, composed of the primary cooling water system and the second cooling water system, is utilized to dissipate the core fission heat. This is achieved through the use of the pulse reactor pool, heat exchanger, cooling tower, and heat trap, with forced circulation also being implemented (refer to Figure 1). The XAPR device is characterized by excellent inherent safety, broad applicability, a straightforward structure, as well as an ease in operation and maintenance. The XAPR can operate in a steady mode, with a steady-state operational capacity of 2 MW, as well as in pulse or square wave modes.

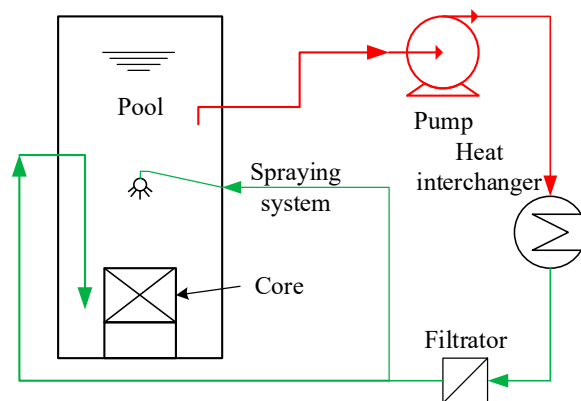


**Figure 1.** Schematic diagram of the XAPR primary circuit.

The steady-state core layout of the XAPR is depicted in Figure 2 [17]. The core is composed of a total of 211 channels distributed across 9 circles, with the central water cavity occupying the center and the control rod occupying 6 channels. Within the core, there are 99 channels occupied by standard fuel elements and 2 channels designated for temperature-measuring fuel elements. Additional core components consist of graphite elements, steady-state control rods, pulse control rods, neutron source elements, absorber elements, and other relevant constituents. Notably, two thermometric fuel elements, denoted as C10 and D2 in Figure 2, are utilized to monitor the core temperature at the peak of steady-state and pulse operation power. The thermometric fuel elements employ the same fuel structure as the standard fuel elements, with the exception of three small holes, which are inclined at a 45° angle, are 1.6 mm in diameter, and located in the center of the fuel core. The hot ends of the three thermocouples are inserted into the bottom of the holes, and are drawn upwards through grooves on the upper graphite core column surface.

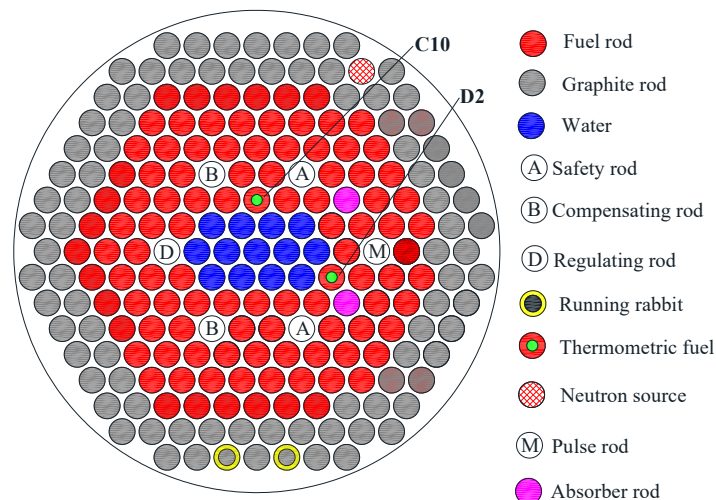


Figure 2. The steady core layout of the XAPR.

The standard fuel element holds significant importance as a key component and core technology within the XAPR. The fuel element uses  $UZrH_{1.6}$ —which is evenly mixed with uranium metal and zirconium hydride—as the fuel, so it is also called the fuel-moderator element. The essential parameters of the fuel element are detailed in Table 1. Due to the utilization of this fuel composition, the core exhibits a substantial instantaneous negative temperature coefficient, endowing the XAPR with a distinct inherent safety characteristic. A depiction of the standard fuel element structure is presented in Figure 3, wherein the fuel rod is filled with helium at a pressure of 0.1 MPa. This helium filling enhances the heat conduction performance between fuel pellets and cladding in addition to facilitating component sealing inspections.

Table 1. The parameters of the XAPR fuel assembly.

Parameter	Units	Value
Pitch	mm	43
Outer diameter	mm	37.2
Inner diameter of pellets	mm	4.6
Outer diameter of pellets	mm	36.1
Cladding thickness	mm	0.5
First-core uranium inventory	%	12
Enrichment of $^{235}U$	%	19.75
Core active zone height	mm	390

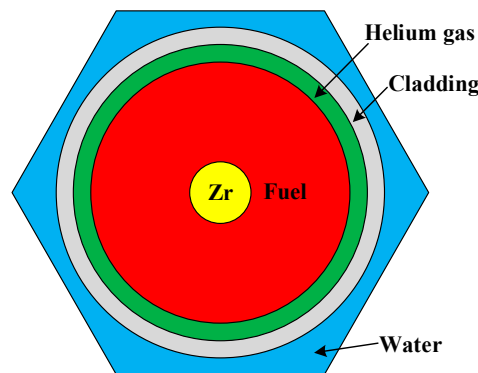


Figure 3. Schematic diagram of the XAPR fuel assembly.

### 3. Models

The steady-state analysis model of the XAPR encompasses the OpenMC neutron calculation model, a three-dimensional fuel-rod heat conduction model, and a coolant parallel multi-channel model [18,19]. The neutronics and thermal-hydraulics coupling analysis model of the XAPR is mainly concerned with data transfer and grid mapping.

#### 3.1. OpenMC Neutronics Model

This paper is founded on the utilization of the OpenMC program, an all-encompassing Monte Carlo software that was devised by the MIT Computational Reactor Physics Group. The OpenMC model adopts a Constructive Solid Geometry (CSG) framework, which enables an accurate representation of the geometric configuration of the reactor core, thereby diminishing the need for the approximations that are employed in equivalent geometric methodologies. The underlying solution strategy of OpenMC involves the resolution of the neutron transport equation through extensive particle sampling. By ensuring an adequate number of samples, the program is capable of effectively reproducing the authentic physical processes. The Monte Carlo method, being a probabilistic statistical approach, facilitates the simulation and statistical analysis of the true trajectory history of neutrons, thereby allowing for the derivation of pertinent physical parameters. The simulation procedure is summarized as follows: Establishing the authentic trajectory history of an individual neutron within a prescribed geometric structure. By tracing a considerable number of neutron histories and accumulating a sufficient number of samples, the eigenvalue of a random variable can be determined via statistical techniques, thus serving as a solution to the underlying problem. The Monte Carlo method offers the advantage of capturing the characteristics of random entities and reflecting the physical processes, while also enables a refined geometric modeling. However, it is accompanied by a relatively lower computational efficiency and inherent statistical errors. In this paper, the neutron calculation model of the XAPR—grounded in OpenMC—is established, as illustrated in Figure 4.

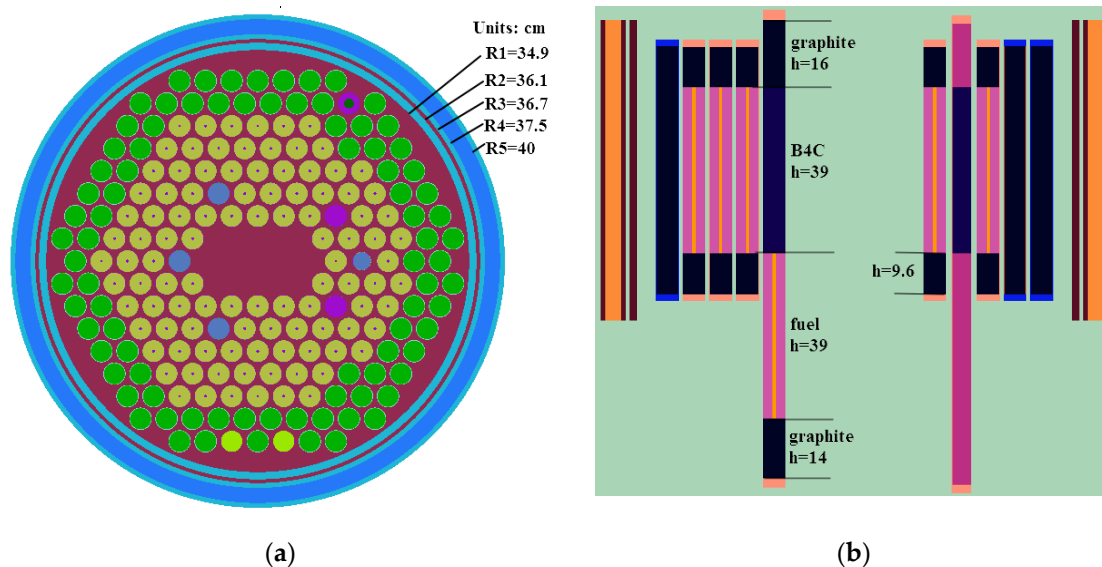


**Figure 4.** The CSG geometry of Xi'an Pulse Reactor: (a) Radial section (XY); (b) axial section (XZ).

The fundamental objective of the OpenMC neutron transport calculation is to depict and analyze the historical development of neutron generation within the system until their eventual disappearance, enabling the derivation of continuous neutron distribution at any given point within the Constructive Solid Geometry (CSG) framework. Conversely, the heat conduction of the fuel and fluid calculations of coolant are typically resolved through

the finite element method. The FEM endeavors to acquire solutions across the entirety of the physical domain through the approximation of the discretized problem. By virtue of its capacity to handle intricate geometric configurations, the FEM is particularly well suited for addressing heat-conduction problems. Consequently, a challenge arises when coupling the OpenMC neutron computation model with the thermal-hydraulic computation model, thus necessitating the resolution of grid mapping and data-transfer concerns.

In this study, a solution is proposed by employing the OpenMC unstructured grid tally function to directly compute the power distribution of the fuel rods within an unstructured grid. This grid was divided axially to ensure consistency with the thermal-hydraulic axial grid, thereby facilitating grid mapping and data transfer in conjunction with the thermal-hydraulic domain. The division scheme for the OpenMC fuel-rod fission power grid is depicted in Figure 5. Additionally, the OpenMC fluid partial count grid model, as presented in Figure 6, was utilized. Thermal-hydraulic feedback was established by utilizing the average temperature and density parameters of the grid elements, which were then employed to inform the neutron calculation process.

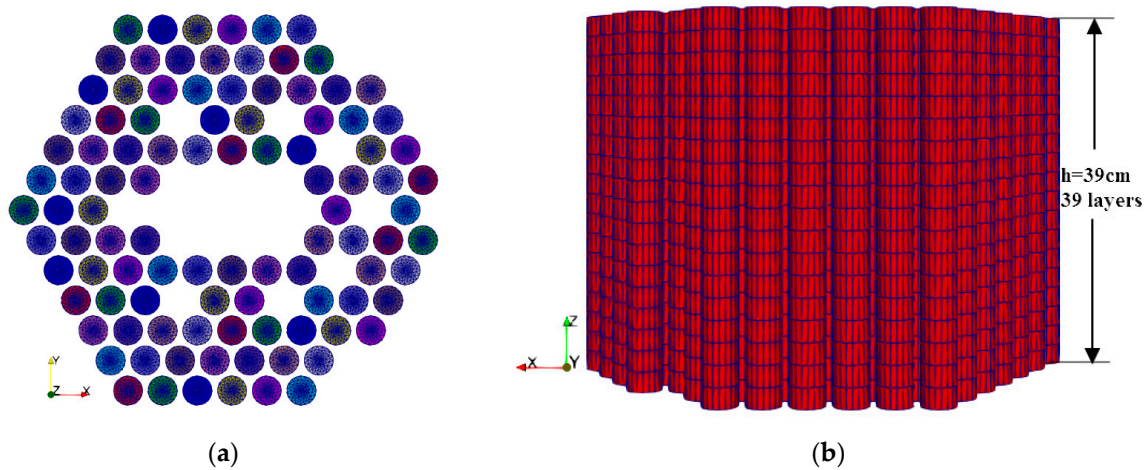


**Figure 5.** Unstructured mesh for the fission heat tally of the fuel rods: (a) Radial section (XY); (b) axial section (XZ).

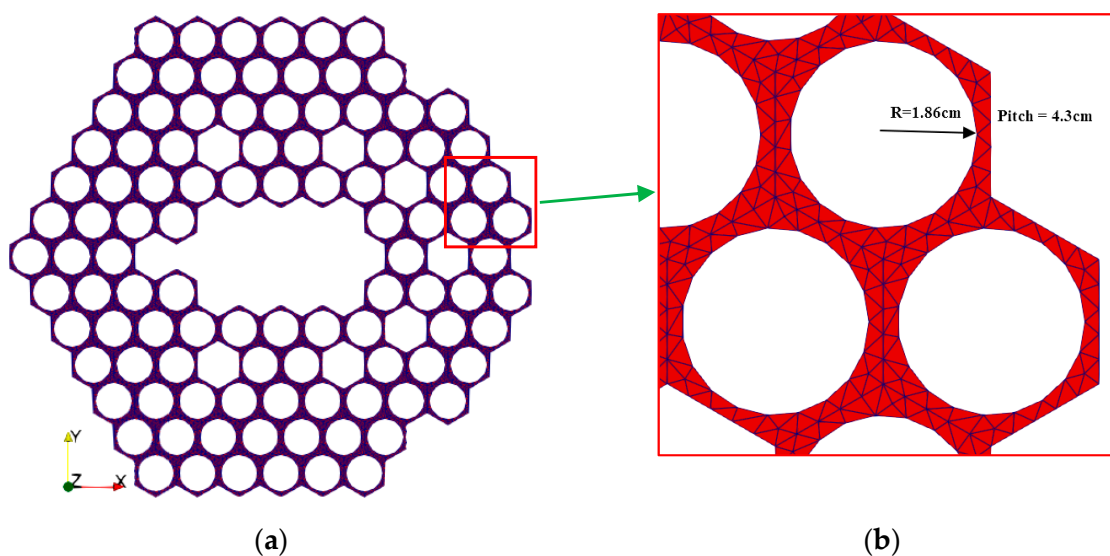


**Figure 6.** Unstructured mesh for the fluid tally: (a) Radial section (XY); (b) partial enlarged drawing.

### 3.2. Fuel Rod Heat Conduction Model

The fuel element utilized in the XAPR system is characterized by a coarse rod configuration, and its XYZ geometry is visually depicted in Figure 7.

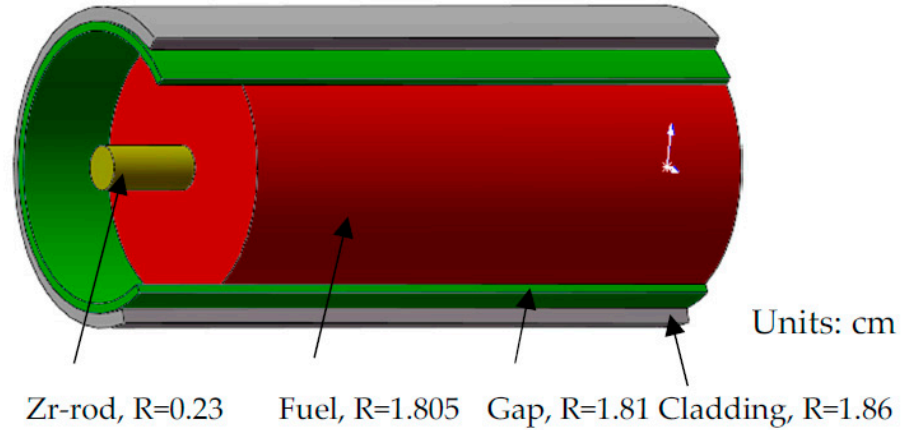


**Figure 7.** The fuel element shape of the XAPR.

Based on the representation provided in Figure 7, the steady-state heat conduction equation for each component of the fuel element can be deduced in the following manner:

1. Heat conduction equation of the Zr rod:

$$\frac{d}{dx}k_{zr}\frac{dT_{zr}}{dx} + \frac{d}{dy}k_{zr}\frac{dT_{zr}}{dy} + \frac{d}{dz}k_{zr}\frac{dT_{zr}}{dz} = 0 \quad (1)$$

2. Heat conduction equation of the fuel pellets:

$$\frac{d}{dx}k_{fuel}\frac{dT_{fuel}}{dx} + \frac{d}{dy}k_{fuel}\frac{dT_{fuel}}{dy} + \frac{d}{dz}k_{fuel}\frac{dT_{fuel}}{dz} + q_v = 0 \quad (2)$$

3. Heat conduction equation of the cladding:

$$\frac{d}{dx}k_{clad}\frac{dT_{clad}}{dx} + \frac{d}{dy}k_{clad}\frac{dT_{clad}}{dy} + \frac{d}{dz}k_{clad}\frac{dT_{clad}}{dz} = 0 \quad (3)$$

where the calculation of the heat source  $q_v$  is performed by utilizing the OpenMC neutronics model.

$$q_v = q_v(x, y, z) \quad (4)$$

In the aforementioned equations,  $\rho$  ( $\text{kg}/\text{m}^3$ ) represents the density,  $k$  ( $\text{W}/(\text{m}\cdot\text{K})$ ) signifies the heat conductivity,  $T$  (K) represents the temperature, and  $q_v$  ( $\text{W}/\text{m}^3$ ) refers to the volume power density.

In the present analysis, it was assumed that the gap retains a consistent thermal conductivity across various temperature ranges, with a specific value of  $15,019 \text{ W}/(\text{m}^2\cdot\text{K})$  [20]. Moreover, during the heat transfer process within the gap, it was observed that the temperature of both the outer surface of the pellets and the cladding remained relatively low. Consequently, the contribution of radiation heat transfer within the gap could be disregarded.

In the context of heat transfer, the boundary between the fuel cladding and the coolant water was treated such that the temperature was equated to the water temperature that was derived from the fluid heat-transfer calculations. Conversely, all other surfaces were considered to possess adiabatic boundary conditions. To facilitate a three-dimensional heat conduction calculations for the fuel rods, the grid depicted in Figure 8 was employed.

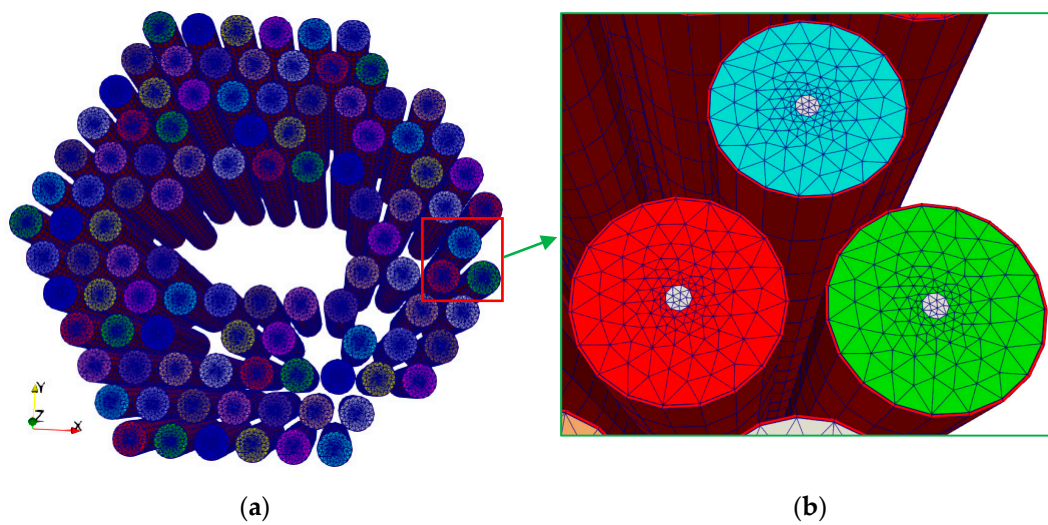


**Figure 8.** Mesh for the heat transfer simulation of the fuel rods: (a) Global view; (b) partial enlarged drawing.

The fundamental properties of the fuel rod are presented in Table 2 [4,21].

**Table 2.** The fundamental properties of the fuel rod.

Property	Units	Materials	Value/Expression
Density	g/cm <sup>3</sup>	Fuel	6.1792
		Zr-rod	6595.2 − 0.1477T
		Cladding	7.9
		Water	264.756 + 6.47282T − 0.01788T <sup>2</sup> + 1.478 × 10 <sup>−5</sup> T <sup>3</sup>
Thermal conductivity	W/(m·K)	Fuel	19.70941 − 0.01482T + 2.8764 × 10 <sup>−5</sup> T <sup>2</sup> − 9.38889 × 10 <sup>−9</sup> T <sup>3</sup>
		Zr-rod	7.51 + 0.0209T − 1.45 × 10 <sup>−5</sup> T <sup>2</sup> + 7.67 × 10 <sup>−9</sup> T <sup>3</sup> , T: °C
		Cladding	373 K: 16.329; 573 K: 18.841; 773 K: 22.19
		Water	−1109.13 + 11.4T + 0.02377T <sup>2</sup> − 1.62 × 10 <sup>−5</sup> T <sup>3</sup> , (103 W/m·K)

### 3.3. Parallel-Channel Fluid Model of the XAPR

The XAPR fuel operates by generating heat through the process of fission, which is subsequently transferred through the fuel-pellets’ gap cladding via heat conduction. This heat is then transferred to the interface between the coolant and containment through natural convection. In this study, a steady-state thermal-hydraulic model of the core was employed via utilizing a parallel multi-channel approach. This model neglects the heat and mass transfer between neighboring fuel channels and assumes that the amount of heat carried by the fluid per unit of time is equal to the heat generated within the fuel. This modeling approach is illustrated in Figure 9. The axial temperature distribution of the fluid was determined by solving the following energy conservation equation:

$$c_p \dot{m} \Delta T(z) = \dot{q}(z) \tag{5}$$

In the given equation,  $c_p$  represents the specific heat capacity at constant pressure,  $\dot{m}$  denotes the mass flow rate of water, and  $\dot{q}$  represents the line power density.

The XAPR represents a pool reactor design that relies on the core’s natural circulation for cooling, wherein the flow of coolant is contingent upon the disparity between the fuel

cladding and the coolant water. The formula for the natural circulation flow can be derived by integrating the momentum conservation equation along the axial axis.

$$\sum_{i=1}^n \frac{l_i}{A_i} \cdot \frac{dW}{dt} + \sum_{i=1}^n \left( \frac{f_i l_i}{D_{e,j}} + K_i \right) \frac{W^2}{2\rho_i A_i^2} + \sum_{i=1}^n \int_{l_i} \rho_i g dl_i = 0 \quad (6)$$

where  $A$  represents the area of the flow channel,  $f$  denotes the frictional coefficient,  $K$  represents the profile drag coefficient,  $l$  represents the length of the flow channel, and  $W$  denotes the fluid mass flowrate.

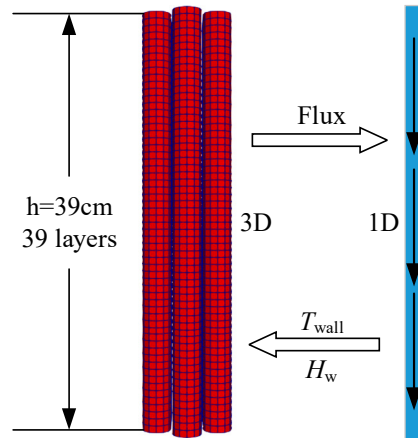


**Figure 9.** The diagram of the flow–solid coupling data transfer.

Based on the aforementioned equation, a self-developed computational code was employed to compute the fluid mass flowrate values of approximately 11.91 kg/s for the XAPR [22]. In a separate study, Zhao et al. utilized the RELAP5 code to obtain the fluid mass flowrate values of roughly 12.13 kg/s for the XAPR [23]. Furthermore, the designated value for the natural circulation fluid mass flowrate in the XAPR design stands at 12.13 kg/s, accompanied by a corresponding velocity of 0.204 m/s. In this study, the design value was chosen as the reference. To calculate the Nusselt number ( $Nu$ ), the Gnielinski relation was selected.

$$Nu = 0.012 \left( Re^{0.87} - 280 \right) Pr^{0.4} \left[ 1 + \left( \frac{d}{l} \right)^{2/3} \right] \left( \frac{Pr_f}{Pr_w} \right)^{0.11} \quad (7)$$

where  $d$  is hydraulic diameter,  $l$  is the length of the flow channel, and suffixes of  $f$  and  $w$  represent fluid and wall temperature, respectively.

### 3.4. Coupling Method of the XAPR

In this paper, the computation of the neutron transport was carried out using the OpenMC program within the Cardinal framework. The Cardinal serves as an external interface of MOOSE, enabling seamless integration and coupling calculations with other MOOSE programs. The coupled solution of the neutronics and thermal-hydraulic models was attained through the utilization of the MultiApp and Transfer functions that are integrated within MOOSE. As illustrated in Figure 10, the multi-physics coupling scheme adopts the OpenMC-based Monte Carlo computing approach as the MultiApp. This MultiApp encompasses 101 SubApps that are dedicated to the calculation of the three-dimensional heat conduction within the fuel rods. Notably, each SubApp incorporates a fluid computations component. The Transfer function offered by MOOSE effectively facilitates the exchange in data between the MultiApp and the SubApps.

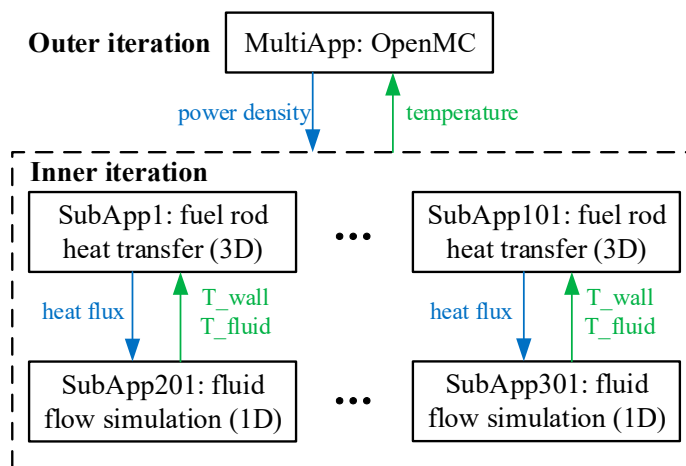


Figure 10. Scheme for multi-physics coupling.

The flow of the steady-state neutronics and thermal-hydraulic coupling calculations for the XAPR is presented in Figure 11. The computation begins by utilizing OpenMC to perform the neutron transport analysis for the entire core of the XAPR. The resulting core power density is then converted into a heat source, which is subsequently used for the heat conduction calculation of the fuel rod. The temperature distribution within the fuel is fed back into the neutron model, thus enabling the interpolation of new fuel cross-sections. This process is iteratively repeated for subsequent rounds of calculation. Moreover, the heat flux originating from the outer boundary of each fuel rod is transferred to the corresponding one-dimensional fluid model as a boundary condition. The resulting temperature distribution is again fed back into the neutron model, allowing for the interpolation of new coolant cross-sections. This iterative procedure continues using the Picard iteration until convergence is achieved and the calculation is concluded.

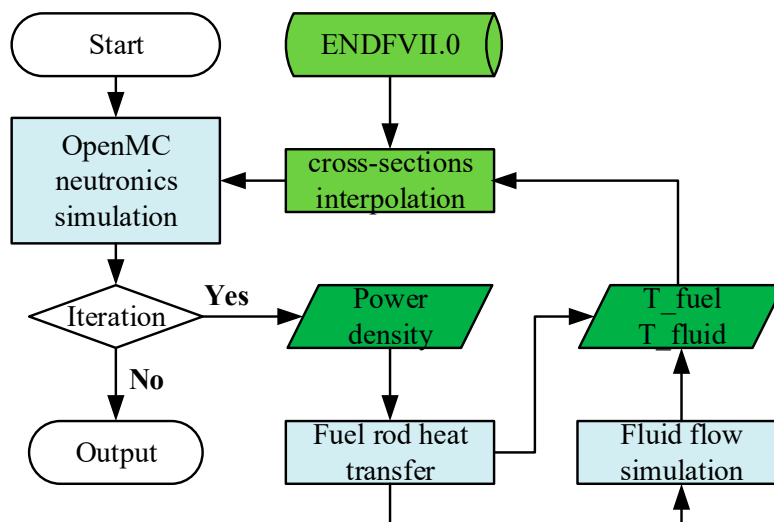


Figure 11. Steady-state calculation flow chart of the XAPR.

#### 4. Numerical Results

In this study, the established physical model and coupling scheme, as described in the third section, were applied to perform the neutronics and thermal-hydraulic coupling calculations of the steady-state 2 MW XAPR core. Firstly, the convergence of the Picard iteration was analyzed to ensure the reliability of the computational approach. Subsequently, the core power distribution, fuel temperature distribution, and coolant temperature distribution were determined and presented as the outcomes of the calculation process.

### 4.1. Convergence Analysis

In the OpenMC neutron calculation, 100,000 particles were utilized per generation, with 100 generations designated as inactive batches and 400 as active batches. For the heat conduction calculation of the fuel rods, the relative error was set at  $1 \times 10^{-8}$ , the relative error for the Picard iteration was  $1 \times 10^{-4}$ , and the relative error for the fluid calculation was  $1 \times 10^{-5}$ .

Figure 12 presents the variations in the eigenvalue  $k_{eff}$  with each iteration step, while Figure 13 depicts the changes in the maximum temperature values of the fuel and coolant during the Picard iteration process. As evident from Figures 12 and 13, the coupling calculation concludes after 12 iterations of the Picard method. At the second step of the Picard iteration, the relative eigenvalue  $k$  stabilizes with minimal fluctuation. This behavior can be primarily attributed to the limited alterations in the fuel and coolant temperatures, which exhibit negligible changes within the 2–12 iteration range (approximately 8 K and 0.6 K, respectively). Consequently, the material cross-sections remained confined within this range. The obtained results unequivocally demonstrate the rapid convergence of the established neutronics and the thermal-hydraulic coupling calculation scheme that is proposed in this paper.

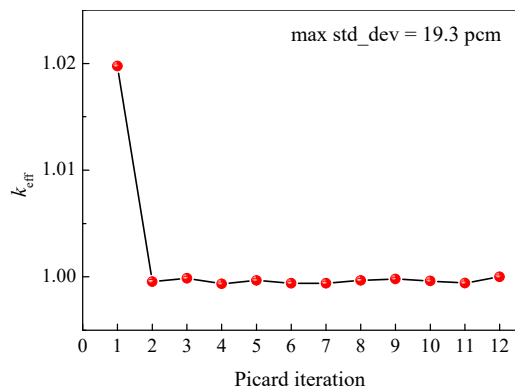


Figure 12. The  $k_{eff}$  vs. the iteration number.

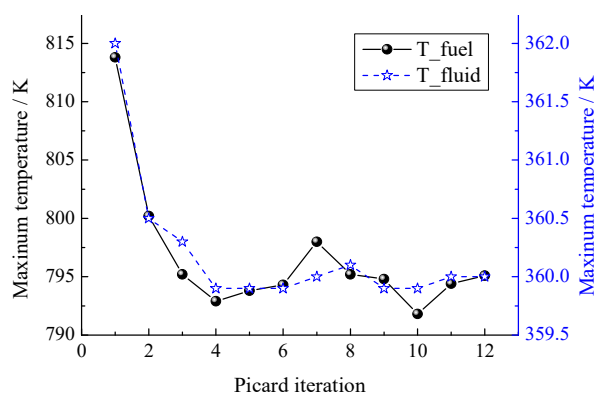
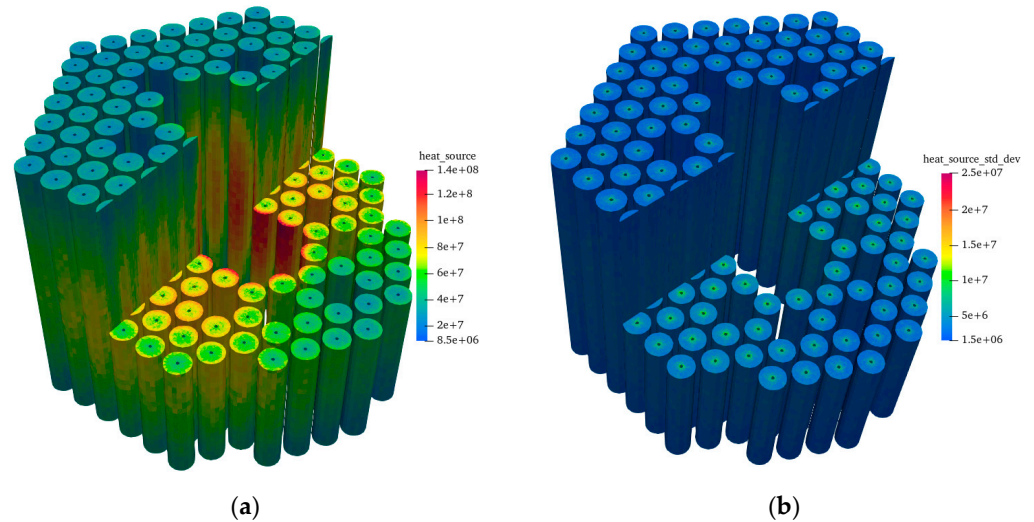


Figure 13. The maximum temperature vs. the iteration number of the fuel and fluid.

### 4.2. Coupling Method of the XAPR

This study employs the previously established multi-physical coupling scheme to calculate the principal steady-state parameters of the XAPR. Figure 14 illustrates the resulting core power distribution. An analysis of Figure 14 revealed that the power density in the fuel element ring that surrounds the central water cavity was notably high. This occurrence can be attributed primarily to the moderating influence of the central water cavity on the neutrons. Furthermore, it is evident that the self-screening effect of the fuel

rod was pronounced, with the external power of the fuel core surpassing the internal power. Moreover, the statistical deviations were more significant in regions where the internal power is relatively low.



**Figure 14.** (a) Power density distribution of the XAPR; (b) standard deviation of the power density distribution of the XAPR.

Figure 15 presents the distribution of the temperature within the core fuel rods, while Figure 16 displays the distribution of the coolant temperature. The maximum temperature of the core fuel, which corresponds to the peak temperature of the C10 thermometric fuel element, was reported as 843 K. Simultaneously, the temperature recorded at the outlet of the thermal channel was measured at 370 K. In this study, calculations revealed that the highest temperature within the C10 thermometric fuel element reached 795.1 K, resulting in a deviation of approximately  $-5.7\%$  from the measured value. Moreover, the temperature at the outlet of the thermal channel was determined to be 360.0 K, exhibiting a deviation of around  $-2.7\%$  from the measured value.

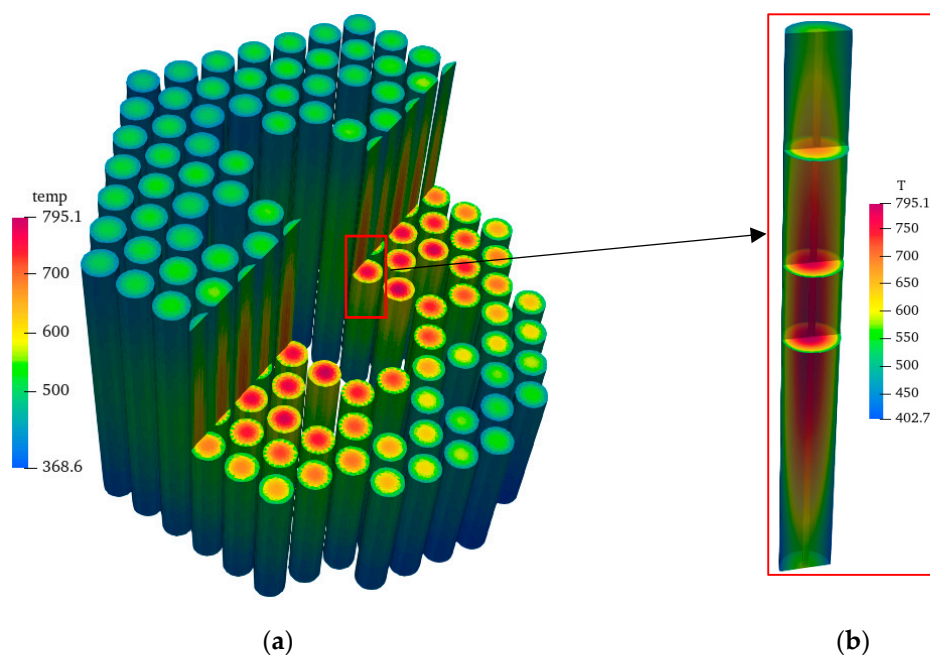


**Figure 15.** Temperature distribution of the XAPR: (a) the core; (b) the C10 rod.

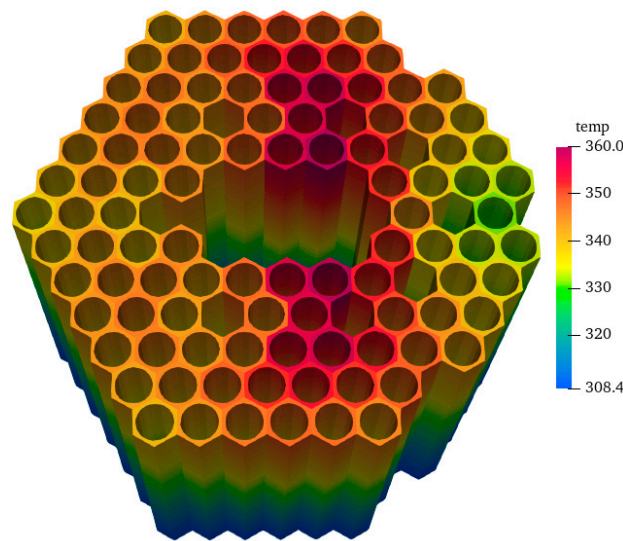


**Figure 16.** Temperature distribution of the fluid in the XAPR.

The radial mean temperature distribution of the coolant thermal channel is presented in Figure 17. An analysis of Figure 17 revealed that the coolant water experiences gradual heating as it progresses through the channel, while the fuel cladding wall temperature undergoes continuous cooling. This behavior can be attributed to the high power density and the increasing fluid temperature along the inlet distance. Consequently, the fuel temperature attains its maximum value near the mid-plane.

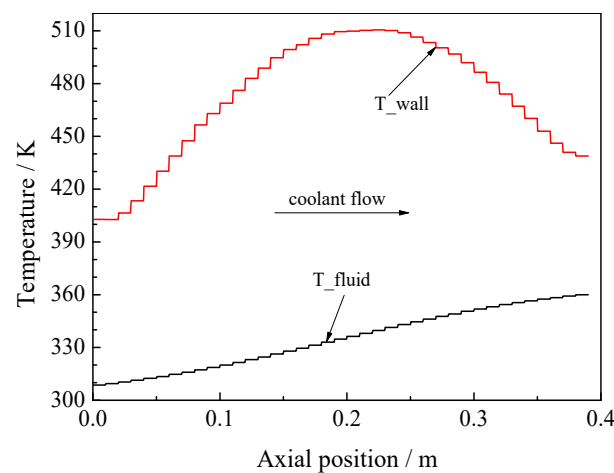


**Figure 17.** Radially averaged temperatures as a function of the C10 rod axial position.

## 5. Conclusions

Through utilizing the Cardinal multi-physical coupling framework, this study investigated the steady-state power distribution and temperature distribution of the XAPR by employing the internal coupling method of OpenMC and thermal-hydraulic calculations. The three-dimensional power distribution of the fuel rods was obtained through the implementation of the OpenMC's unstructured grid counting function. Subsequently, by integrating the three-dimensional heat conduction calculation model of the fuel rods and the multi-channel model of the coolant in parallel, the internal coupling calculations of various physical models were achieved via the MultiApp and Transfer functions of the MOOSE framework. As a result, the three-dimensional power distribution, fuel temperature, and fluid temperature distribution under steady-state conditions for the XAPR were determined.

Based on the calculations, the highest temperature recorded by the C10 thermometric fuel element was 795.1 K, exhibiting a deviation of approximately 5.7% from the measured value. Additionally, the temperature recorded at the outlet of the thermal channel was determined to be 360.0 K, with a deviation of roughly  $-2.7\%$  from the measured value. Within the given error range, the calculated values aligned well with the measured values, thereby indicating that the established neutronics and thermal-hydraulic coupling calculation scheme effectively simulated the steady-state operational conditions of the XAPR. Based on the results obtained, some suggestions are listed as follows:

- (1) The steady-state condition of the XAPR denotes a safety limit for the fuel core temperature, and this was established at 913 K. Notably, the maximum temperature recorded for the fuel element in the XAPR was 795.1 K, with a sufficient margin of safety distance. Furthermore, the XAPR is equipped with a comprehensive core temperature monitoring system that facilitates the real-time tracking of temperature fluctuations. If the temperature exceeds the prescribed limit, the protection system is automatically activated to ensure the secure operation of the reactor.
- (2) Notably, since the XAPR operates as a thermal neutron reactor with minimal fuel rod deformations that could result from thermal expansion, this study did not consider the influence of fuel element deformations on the neutron calculations. However, future investigations can explore the impact of geometric deformations that arise from mechanical effects on neutronics calculations.
- (3) The examination of fuel burnup assumes a critical role in the safety assessment of the reactor. As the reactor's fuel burnup advances, the physical characteristics of the reactor core manifest alterations. Consequently, it is imperative to undertake a comprehensive investigation of the numerical anomalies arising from burnup-induced power transfers within the XAPR model as part of future research endeavors.

**Author Contributions:** Conceptualization, Methodology, Investigation, Writing—Original Draft, D.J.; Resources, Writing—Review and Editing, Data Curation, P.X.; Validation, Formal analysis and Visualization, T.H.; Resources, Writing—Review and Editing, Supervision, X.J.; Validation and Experiment, L.W.; Resources and Review, D.L.; Writing—Review, Experiment, X.Z.; Validation and Visualization, L.C. All authors have read and agreed to the published version of the manuscript.

**Funding:** This research was funded by the National Natural Science Foundation of China, grant numbers 12205237 and 12275219.

**Data Availability Statement:** The data presented in this study are available on request from the corresponding authors. The data are not publicly available due to privacy.

**Conflicts of Interest:** The authors declare no conflict of interest.

## References

1. Ebyan, O.A.; Khamis, H.A.; Baghdady, A.R.; El-Feky, M.G.; Abed, N.S. Low-temperature alteration of uranium–thorium bearing minerals and its significance in neoformation of radioactive minerals in stream sediments of Wadi El-Reddah, North Eastern Desert, Egypt. *Acta Geochim.* **2020**, *39*, 96–115. [[CrossRef](#)]
2. Okasha, S.A.; Faheim, A.A.; Monged, M.H.E.; Khattab, M.R.; Abed, N.S.; Salman, A.A. Radiochemical technique as a tool for determination and characterisation of El Sela ore grade uranium deposits. *Int. J. Environ. Anal. Chem.* **2023**, *103*, 737–746. [[CrossRef](#)]
3. Taha, S.H.; Sallam, O.R.; Abbas, A.E.A.; Abed, N.S. Radioactivity and environmental impacts of ferruginous sandstone and its associating soil. *Int. J. Environ. Anal. Chem.* **2021**, *101*, 2899–2908. [[CrossRef](#)]
4. Chen, W.; Jiang, X.; Chen, L.; Yuan, J.; Zhang, L.; Zhu, Y.; Zhang, X. *Physical and Safety Analysis of the UZrH Pulse Reactor*; Science Press: Beijing, China, 2018.
5. Jiang, X.; Wu, Z.; Su, C.; Zhang, W.; Yu, Q. Thermal neutron source design for nuclide parameter measurement with on-line prompt gamma ray method. *At. Energy Sci. Technol.* **2019**, *53*, 913–919.
6. Guo, H.; Zhao, Z.; Chen, L.; Zhang, X.; Wang, L.; Jiang, X. Coupled calculation method of criticality and burnup. *High Power Laser Part. Beams* **2013**, *25*, 147–149. [[CrossRef](#)]
7. Zhang, H.; Wang, K.; Jiang, X. Development of pulsed reactor thermal hydraulic design codes. *Nucl. Power Eng.* **2002**, *23*, 33–35.
8. Chen, L.; Chen, W.; Zhang, Y.; Jiang, X.; Zhao, Z. Safety analysis for Xi'an Pulsed Reactor in pulse operation mode with the core in steady arrangement and design project for the new core arrangement. *Nucl. Power Eng.* **2006**, *27*, 1–17.

9. Zhao, Z. *Study on the Calculation Method of Space-Time Neutron Kinetics Coupled with Thermal-Hydraulics and Experimental Verification in XAPR*; Northwest Institute of Nuclear Technology: Xi'an, China, 2012.
10. Zhang, X.; Jiang, X.; Zheng, Y.; Wang, Y.; Yin, H.; He, B.; Xu, P.; Wang, L.; Guo, H.; Zhang, L.; et al. Three-dimensional transient analysis of Xi'an pulsed reactor by the coupled neutronics and thermal-hydraulics code. *Ann. Nucl. Energy* **2022**, *175*, 109254. [[CrossRef](#)]
11. Shriwise, P.C.; Zhang, X.; Davis, A. DAG-OpenMC: CAD-based geometry in OpenMC. *Proc. Am. Nucl. Soc. Winter Meet.* **2020**, *122*, 395–398.
12. Wang, J.; Li, Z.; Ding, M. Study of the neutronic and thermal coupling effect on VHTR fuel pebble using OpenMC and OpenFOAM. *Ann. Nucl. Energy* **2023**, *183*, 109643. [[CrossRef](#)]
13. Wang, W.; Feng, W.; Zhang, K.; Yang, G.; Ding, T.; Chen, H. A moose-based neutron diffusion code with application to a LMFR benchmark. In Proceedings of the 23rd Pacific Basin Nuclear Conference, PBNC 2022, Beijing & Chengdu, China, 1–4 November 2022; Volume 1, pp. 490–502.
14. Weiss, A.G.; Zaidan, L.J.; Bani Ahmad, M.T.H.; Abdoelatef, M.G.; Peterson, J.W.; Lindsay, A.D.; Kong, F.; Kimber, M.L.; Ahmed, K. *Characterization of the Finite Element Computational Fluid Dynamics Capabilities in the Multiphysics Object Oriented Simulation Environment*; Idaho National Laboratory: Idaho Falls, ID, USA, 2023.
15. Huxford, A.; Leite, V.C.; Merzari, E.; Zou, L.; Petrov, V.; Manera, A. A hybrid domain overlapping method for coupling System Thermal Hydraulics and CFD codes. *Ann. Nucl. Energy* **2023**, *189*, 109842. [[CrossRef](#)]
16. Novak, A.J.; Andrs, D.; Shriwise, P.; Fang, J.; Yuan, H.; Shaver, D.; Merzari, E.; Romano, P.K.; Martineau, R.C. Coupled Monte Carlo and thermal-fluid modeling of high temperature gas reactors using Cardinal. *Ann. Nucl. Energy* **2022**, *177*, 109310. [[CrossRef](#)]
17. Chen, L. Investigation of Subcooled Boiling Heat Transfer Characteristics and Void Fraction Calculating Method of the Pulsed Reactor. Ph.D. Thesis, Nanjing University of Aeronautics and Astronautics, Nanjing, China, 2012.
18. Gong, H.; Zhang, X.; Gui, N.; Huang, Y.; Yang, X. Study of density wave instability in natural circulation with parallel channels under inclined and heaving conditions. *Prog. Nucl. Energy* **2023**, *155*, 104525. [[CrossRef](#)]
19. Upadhyay, R.; Raghuvanshi, N.S.; Dutta, G. Nuclear coupled thermal-hydraulic analysis of parallel channel density wave instabilities in a supercritical water reactor. *Ann. Nucl. Energy* **2023**, *181*, 109495. [[CrossRef](#)]
20. Jing, C.; Shan, J.; Zhu, J.; Chen, D. Lumped-parameter models for transient conduction in pulse reactor fuel rod. *Chin. J. Nucl. Sci. Eng.* **1999**, *19*, 210–214.
21. Tian, S. The safe character of fuel for pulsed reactor and its utilization in the compact power reactor. *Nucl. Power Eng.* **1991**, *12*, 52–57.
22. Tian, Y.; Chen, S.; Yang, N.; Zhu, L.; Li, H.; Ma, T.; Hu, P.; Kang, X. Transient safety characteristic analysis of Xi'an Pulsed Reactor during reactivity insertion accident. *At. Energy Sci. Technol.* **2020**, *54*, 2089–2097.
23. Zhao, W.; Chen, L.; Liu, G.; Zhang, L.; Yang, N.; Zhang, X.; Tian, X.; Sun, P.; Yuan, J. Multi-scale coupling transient characteristics of Xi'an Pulsed Reactor based on RELAP5 and CTF. *Nucl. Power Eng.* **2023**, *44*, 59–64.

**Disclaimer/Publisher's Note:** The statements, opinions and data contained in all publications are solely those of the individual author(s) and contributor(s) and not of MDPI and/or the editor(s). MDPI and/or the editor(s) disclaim responsibility for any injury to people or property resulting from any ideas, methods, instructions or products referred to in the content.